Journal of Thermal Science Vol.31, No.1 (2022) 47–61

https://doi.org/10.1007/s11630-022-1545-5 **Article ID: 1003-2169(2022)01-0047-15**

Assessment of the Turbulence Characteristics of Shaped Film Cooling Hole with Scale Resolving Simulation

WANG Qingsong, SU Xinrong*, YUAN Xin

Key Laboratory for Thermal Science and Power Engineering of Ministry of Education, Department of Energy and Power Engineering, Tsinghua University, Beijing 100084, China

Abstract: The turbulence characteristics of the shaped hole film cooling are very complex. In this study, Large Eddy Simulation (LES) and Reynolds-averaged Navier-Stokes (RANS) are used to study the film cooling of the shaped hole. The time-averaged results are compared with the experimental data in the literature. Because of the eddy-viscosity model, the RANS method roughly deals with the simulation of boundary layer, which leads to a large deviation. The RANS results are compared with the LES results to identify the weaknesses of the Realizable k-ε model in predicting the turbulence characteristics of the shaped hole film cooling. The eddy viscosity hypothesis and the temperature gradient diffusion hypothesis are evaluated using LES data. Furthermore, the turbulence characteristics of the in-hole flow are analysed with the help of the incremental Proper Orthogonal Decomposition (iPOD). The turbulence presents strong anisotropy and some convection structures are induced from the shear zone.

Keywords: shaped film cooling, turbulence characteristics, les, rans, iPOD

1. Introduction

In order to improve the efficiency of the turbine, the inlet temperature of the turbine continues to rise up to 1700℃ in the future, far exceeding the limit temperature of the turbine material. Therefore, it is necessary to strengthen cooling protection. The application of film cooling has greatly improved the cooling effect, and is now widely used in heavy gas turbines and aero engines. Film cooling is to jet coolant through discrete cooling holes on the surface of the component to form a covering film between the wall and the high-temperature mainstream, thereby protecting the wall from hot gas and extending the life of the component.

There are many factors that affect the performance of film cooling. Bogard and Thole [1] found that the geometry of film holes and wall effect make the turbulence characteristics near the wall of the formed hole very complicated. The understanding of the relevant flow mechanism and heat transfer characteristics is of instructive significance for the cooling configuration design to improve the film cooling effect. In order to obtain more flow field information, the numerical simulation is widely used. Computational Fluid Dynamics (CFD) has been widely used for the flow and heat transfer characteristics [2]. More and more researchers use experiments to verify the results of numerical simulation in their research, and after ensuring its accuracy, make full use of the rich flow field information provided by numerical simulation for flow mechanism analysis. Galeazzo et al. [3] used the particle image tracing method (PIV), Large Eddy Simulation

Article type: Contributed by Asian Congress on Gas Turbines 2020 (August 18–19, 2021, China).
Received: Oct 15, 2021 Corresponding author: SU Xinrong E-mail: suxr@mail.tsinghua.edu.cn

Nomenclature

D	diameter of the cooling hole/m
f	frequency/Hz
k	turbulent kinetic energy/$m^2 \cdot s^{-2}$
M	blowing ratio
Pr_t	turbulent Prandtl number
S_{ij}	strain-rate tensor/s^{-1}
Tu	turbulent intensity
$\overline{u_i'u_j'}$	Reynolds stress/$m^2 \cdot s^{-2}$
$\overline{u_i'\theta'}$	turbulent heat flux/$m \cdot s^{-1}$
X	Cartesian coordinate system (Streamwise)/m
Y	Cartesian coordinate system (Normal)/m
Z	Cartesian coordinate system (Lateral)/m

Greek symbols

α_t	eddy diffusivity/$m^2 \cdot s^{-1}$
ε	turbulent dissipation rate/$m^2 \cdot s^{-3}$
η	film cooling effectiveness, $(T_\infty - T_{aw})/(T_\infty - T_c)$
θ	non-dimensional temperature, $(T - T_{aw})/(T_\infty - T_c)$
υ_t	eddy viscosity/$m^2 \cdot s^{-1}$
ω_i	vorticity components/s^{-1}

Subscripts

aw	adiabatic wall
c	coolant
∞	mainstream

(LES) and Reynolds-averaged Navier-Stokes (RANS) to study the jet flow. The comparison showed that RANS predicted the velocity field well, but the capture of space distribution and level of turbulence were not as consistent as the LES results and experiments. Laroche et al. [4] studied the flow and heat transfer in the blade cooling scheme through experiments and numerical simulations. They found that the numerical simulation results were very consistent with the PIV measurements, but the RANS model overestimated the heat transfer coefficient, while the RANS/LES hybrid simulation provided the best heat transfer estimates and captured many instable phenomena, which was ignored in RANS. Foroutan and Yavuzkurt [5] used RANS and hybrid unsteady RANS (URANS)/LES simulations to study the flow and heat transfer of a single row of cylindrical film cooling holes. By comparing the experimental data and numerical simulation results, they found that compared with RANS, the accuracy of the hybrid unsteady RANS predicting was improved by 40%. From previous numerical simulation studies, it can be seen that although the RANS method has the advantage of low cost, it lacks accuracy. The LES is the opposite. Through scale decomposition simulation, LES can capture a lot of flow field details, which makes the flow field prediction and cooling effect prediction more accurate, but at the same time it improves the requirements for grid refinement and computational cost.

In order to improve its accuracy while taking advantage of the RANS method, some researchers have done some research. Begeles et al. [6] realized the anisotropic turbulence model by multiplying the transverse vortex viscosity by a correction factor that varies according to the wall normal distance and applied it to the jet flow study. The results conform to the turbulent logarithm law. Lakehal et al. [7] proposed a turbulence model based on the known DNS data and boundary layer flow laws. The model included the anisotropy of the turbulent transport coefficient in the transport equation and the turbulent Prandtl number in the near-wall area varied with the local Reynolds number. The validity of the model has been verified by experiments. Bianchini et al. [8] systematically studied the performance of the RANS turbulence model developed for film cooling applications, including the vortex viscosity anisotropy tensor correction model and the unsteady model. The results showed that the model improved the prediction accuracy under low and medium blowing ratios. There was no uniform model that could accurately predict the flow field under all conditions. Ling et al. [9] used machine learning to train the direct numerical simulation (DNS) data of pipeline flow against the anisotropy of Reynolds stress, and repositioned the centre position of drawing the Reynolds stress anisotropy triangle, which effectively improved the prediction accuracy, but each training was only for a specific kind of flow. In order to effectively develop a more accurate turbulence model, it was first necessary to fully understand the turbulence characteristics of film cooling near the wall. Many researchers have used more accurate scale simulation methods such as LES to study film cooling. Sarkar and Babu [10] used LES to analyse various vertical structures in the cross-flow jet field and explained the interaction between horseshoe vortex and kidney vortex (CRVP). Stratton and Shih [11] used LES to predict the film cooling of cylindrical holes, and used the results of LES to evaluate the irrationality of the RANS turbulence model. The results showed that due to the influence of the vortex structure, the hypothesis of vortex viscosity in the near-wall region was not fully established. The turbulent Prandtl number is not constant within a certain range, and this analysis has guiding significance for revising the RANS model.

In this study, LES and RANS are used to study the film cooling of the shaped hole. The LES data is used to evaluate the eddy viscosity hypothesis and the

temperature gradient diffusion hypothesis. Through the comparison of LES and RANS results, the weakness of Realizable k-ε (RKE) model in predicting the film cooling of shaped holes is determined, which is the basis for improving the accuracy of the RKE model. Furthermore, the turbulence characteristics of the in-hole flow are analysed with the help of the incremental Proper Orthogonal Decomposition (iPOD). Through detailed exploration, the flow mechanism of the in-hole flow is investigated, which could inspire the modelling the in-hole flow.

The rest of this paper is organized as follows. The next section introduces the setup of numerical situation and the validation of LES result with experiment. Then the time-averaged and instantaneous results are discussed in detail. Finally, the last section concludes the whole paper.

2. Numerical Method

2.1 LES setup

As shown in Fig. 1(a), the calculation domain is a channel with a rectangular coolant plenum. The cross section of the channel is a rectangle with the area $10D\times6D$. D is the diameter of the cylindrical section of the shaped hole, which equals to 3 mm. The geometry structure of the 777-shaped hole proposed by Schroeder and Thole [12] is shown in Fig. 1(b). A turbulent boundary layer is set at the mainstream inlet as a velocity inlet condition. In order to meet the requirements of grid refinement, the grid in the computational domain is finely refined, the wall y^+ is much smaller than 1, and the x^+ and z^+ near the air film hole are both smaller than 10. The cell number reaches 10.86 million. The boundary conditions of the numerical case are listed in Table 1. The upper surface and the side surfaces of the channel are set as symmetrical planes; the side walls of the plenum are adiabatic sliding walls, and the coolant covering wall is set as adiabatic and non-slip wall. The numerical simulation is conducted in commercial software FLUENT19.5 with LES simulation method. The time step is set as 5×10^{-6} s, which equals to $0.04D/U$. A total of 16 passing periods (one passing period=$50D/U$) are calculated, and the statistical average is performed in the 10 passing periods to obtain the time-averaged result.

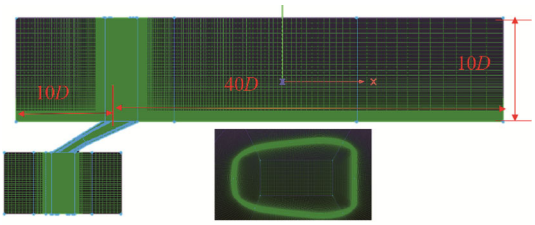

(a) Computational domain

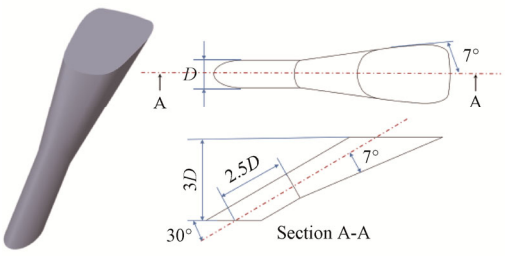

(b) Cooling hole geometry

Fig. 1 Computational domain and 777-cooling hole

2.2 Results validation

As shown in Fig. 2, the lateral-averaged film cooling effectiveness downstream the cooling hole is respectively

Table 1 Boundary conditions

Variable	Value
u_∞	26 m/s
T_∞	328 K
Density ratio	1.2
M	1.0
T_c	273 K
Tu_∞	0.5%
Re_D	4689

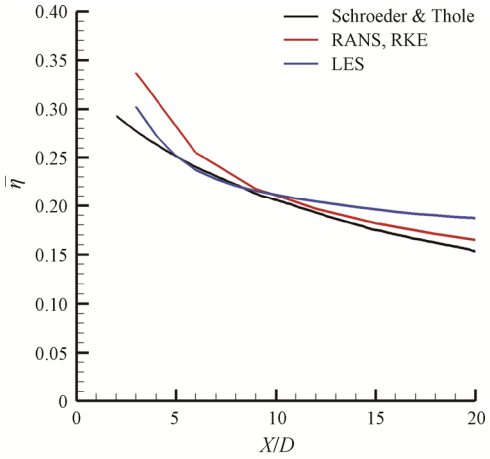

(a) Lateral-averaged results

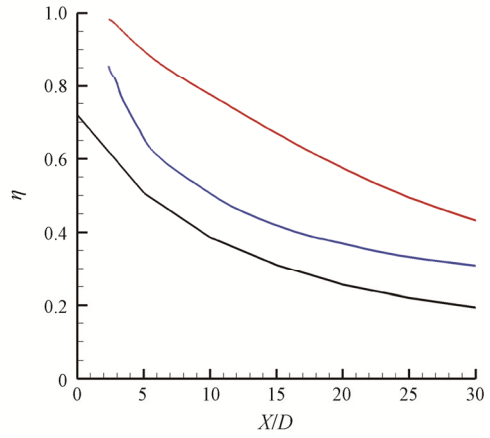

(b) Central line results

Fig. 2 Distribution of film cooling effectiveness

calculated by RANS and the time-averaged results of LES. The results are compared with the experimental data of Schroeder and Thole [12]. The results show that compared to RANS, LES results are more consistent with experimental results, especially not far from the outlet of the shaped hole. At a distance downstream of the air film hole, although RANS results perform better in the lateral-averaged results, it can be seen from the central-line distribution and the contours in Fig. 3 that the RANS results have a higher predictive value of effectiveness on the centre line and a narrower range of coolant diffusion, resulting in the consistence of averaged results, while the LES results are more consistent with the experiment in terms of the central effectiveness and the prediction of the lateral diffusion of coolant. In Fig. 4, by comparing the turbulent boundary layer predicted by the LES results and the RANS results with the experimental results and Spalding Law, it is found that the LES captures the turbulence characteristics more accurately, but the RANS results have larger errors.

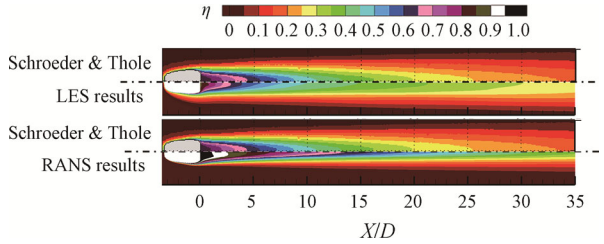

Fig. 3 Adiabatic film cooling efficiency contours

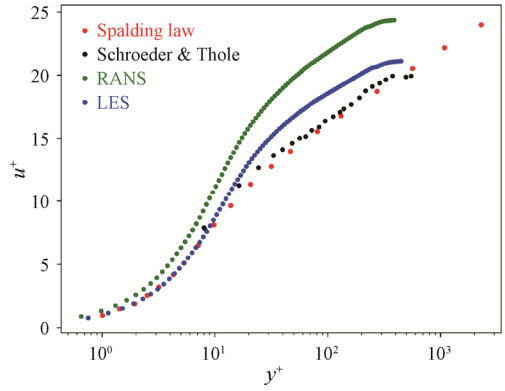

Fig. 4 Turbulent boundary layer velocity distribution

3. Results and Discussion

3.1 Prediction comparison

The film cooling effectiveness and the non-dimensional vorticity contour at X/D=3 are shown in Fig. 5. Compared with the LES results, the RANS results have a wider range with higher effectiveness value near the wall. In terms of vorticity prediction, the core of the CRVP has similar strengths in both prediction but in the RANS results, and CRVP are closer to the wall and smaller in size. The lower position makes the coolant aggregates near the wall; therefore the cooling effectiveness near the wall is higher in RANS results, which also explains the deviation of the cooling effectiveness on the centre line. The smaller size results in a narrower prediction range for coolant diffusion and higher effectiveness downstream, which is corresponding to the effectiveness contour shown in Fig. 3.

Fig. 6 shows the non-dimensional turbulent kinetic energy contours at X/D=3. The results show that the turbulent kinetic energy distribution curvature caused by CRVP can be captured with Realizable k-ε model, but the turbulent kinetic energy value cannot be accurately predicted and tends to be underestimated, especially the turbulent kinetic energy of the jet core near the wall.

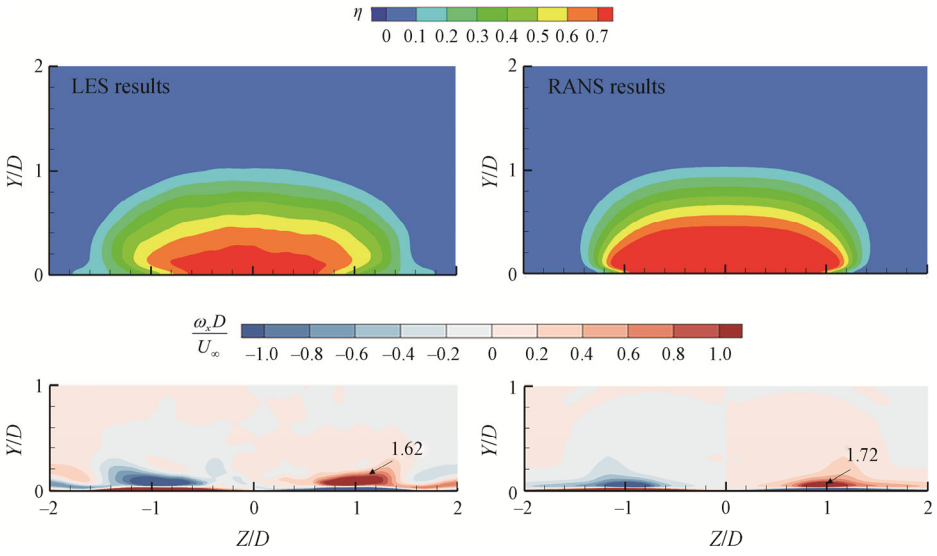

Fig. 5 Cooling effectiveness and non-dimensional vorticity contour at X/D=3

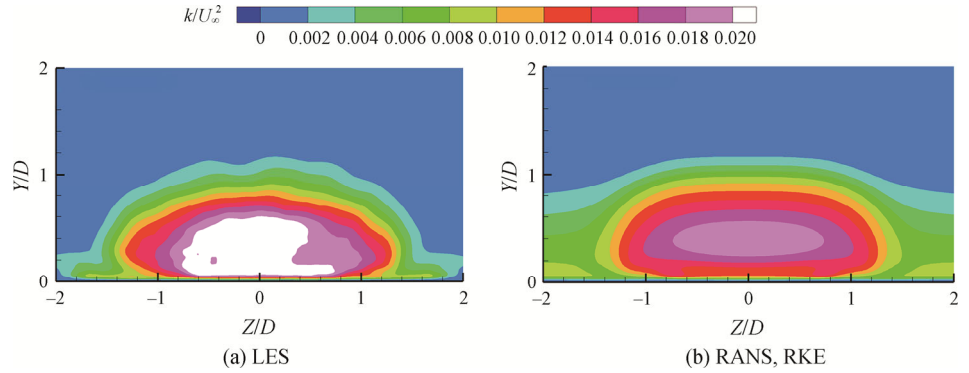

Fig. 6 Non-dimensional turbulent kinetic energy at X/D =3

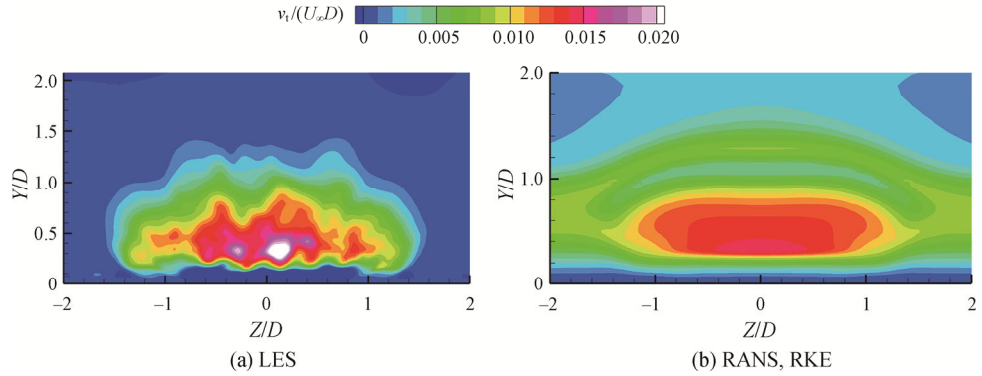

Fig. 7 Non-dimensional eddy viscosity contour at the hole exit

While, that in the mainstream is overestimated. Generally, the distribution of the turbulent kinetic energy in the RANS results is more evenly in contrast to the LES results, and thus the interaction of the mainstream and the coolant is insufficiently predicted in RANS results.

In order to understand the distribution of scalar eddy viscosity intuitively, the least square method is used to calculate the scalar eddy viscosity based on Boussinesq assumption from the LES results according to the Eq. (1):

$$\nu_{\mathrm{tLES}}=\frac{-\overline{u_i'u_j'}\left[S_{ij}-\left(\frac{1}{3}\right)\frac{\partial\overline{u}_{\mathrm{s}}}{\partial X_{\mathrm{s}}}\delta_{ij}\right]+\left(\frac{2}{3}\right)k\delta_{ij}\left[S_{ij}-\left(\frac{1}{3}\right)\frac{\partial\overline{u}_{\mathrm{s}}}{\partial X_{\mathrm{s}}}\delta_{ij}\right]}{2\left[S_{\mathrm{lm}}-\left(\frac{1}{3}\right)\frac{\partial\overline{u}_{\mathrm{s}}}{\partial X_{\mathrm{s}}}\delta_{\mathrm{lm}}\right]^2} \tag{1}$$

where $\overline{u_i'u_j'}$ represents Reynolds stress components; S represents strain-rate tensor; $\frac{\partial\overline{u}_{\mathrm{s}}}{\partial X_{\mathrm{s}}}$ represents the sum of the gradients of the mean velocity components; δ represents Kronecker function, and i, j, l, m are iterated in {1, 2, 3},which respectively represents x, y, z direction.

Fig. 7 shows the non-dimensional scalar eddy viscosity contour of the LES and RANS results. The LES results show that the eddy viscosity near the wall is extremely low while the eddy viscosity at the core of the jet is relatively large. The Realizable k-ε model does not have sufficient prediction of the spatial distribution profile of eddy viscosity. The eddy viscosity near the wall is predicted too high and that at the core of the jet is underestimated. Similar to the turbulent kinetic energy, the distribution of the eddy viscosity in RANS results is more evenly instead of aggregating in the core of jet in LES results. To analyse the in-hole flow, four slices are chosen as shown in the Fig. 8. From the turbulent kinetic energy contour shown in Fig. 9, it can be seen that the concentration characteristics of the turbulent kinetic energy in the separated bubble region are not accurately predicted by RANS, while that in other regions is overestimated. The same phenomenon occurs in the eddy viscosity contours in Fig. 10. As the flow reattached to the wall, the prediction of RANS is gradually similar to LES.

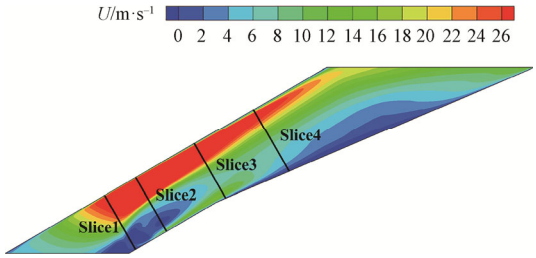

Fig. 8 Positions of the slices chosen in-hole

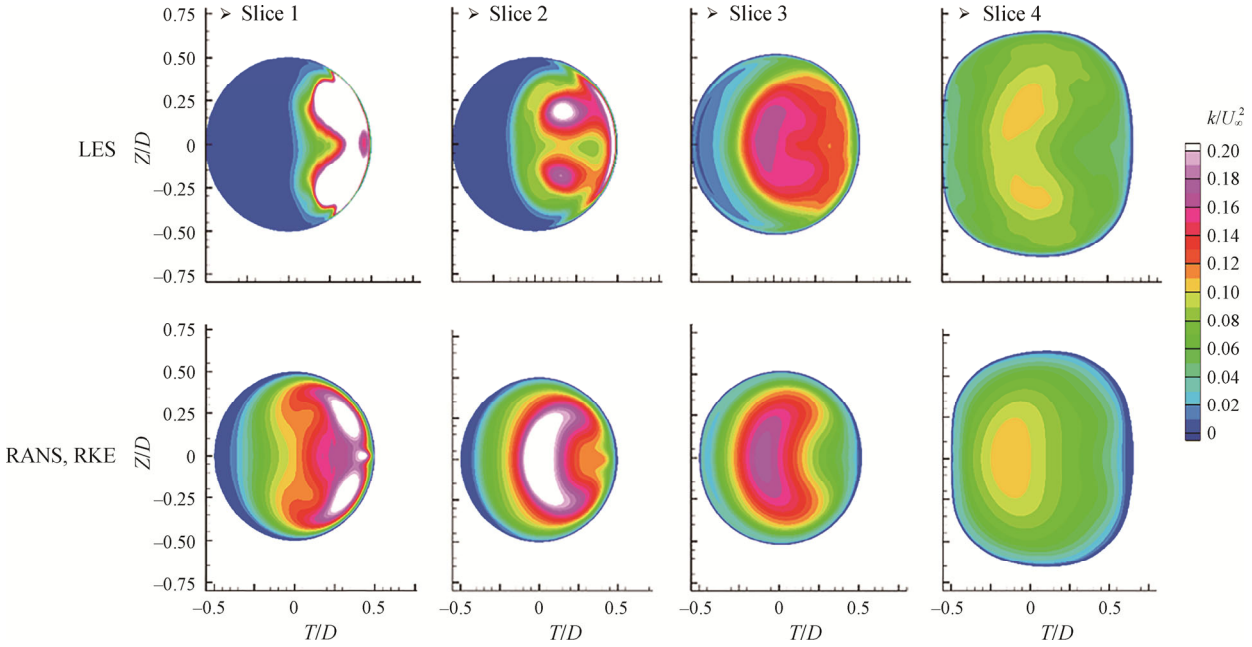

Fig. 9 Non-dimensional turbulent kinetic energy in the shaped hole

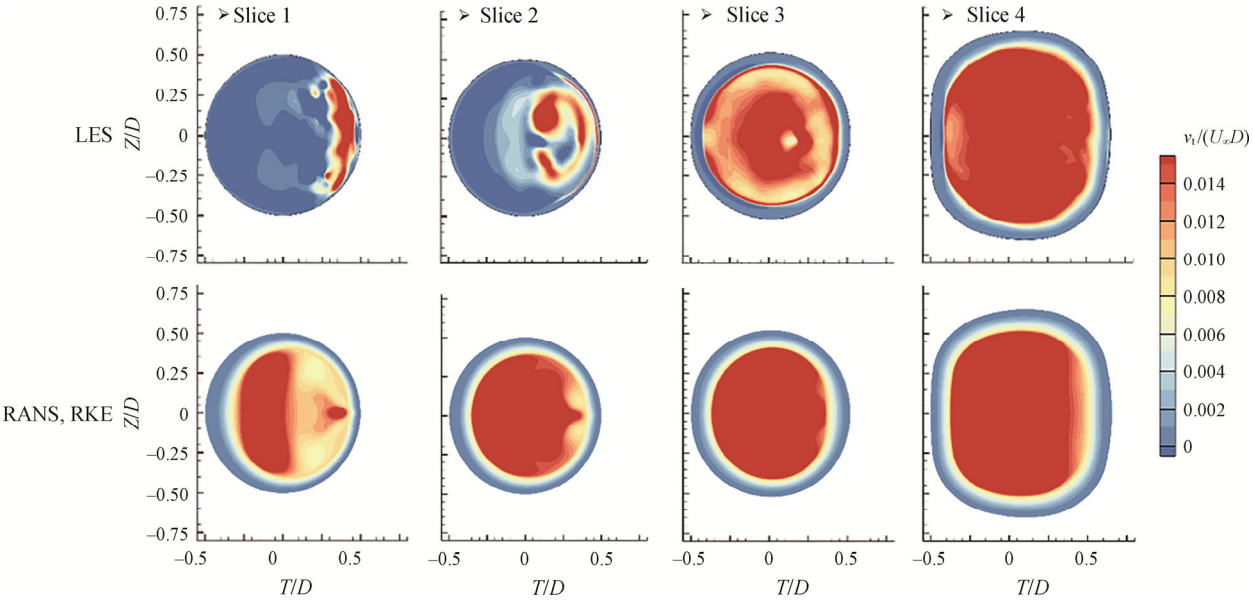

Fig. 10 Non-dimensional eddy viscosity contour in the shaped hole (Upper: LES, Lower: RANS, RKE)

3.2 Evaluation of the Boussinesq hypothesis

Boussinesq hypothesis describes the linear relationship between Reynolds stress and strain, which is the main assumption used in the Realizable k-ε turbulence model. This assumption includes eddy viscosity, which is a function of k and ε, and is used to determine the Reynolds stress. The validity of the linearity assumption can be evaluated by drawing the distribution of stress and strain using LES data and qualitatively checking whether the scalar eddy viscosity is appropriate. If the linear relationship holds, the stress and strain distributions should match, although the magnitudes may be different. Fig. 11 and Fig. 12 show the stress and strain contour of shear stress in different directions, where blue represents negative values and red represents positive values. Since the eddy viscosity is always positive, the colours in the corresponding contours should be the same. It can be seen from Fig. 11 that when Y/D>0.1, the shear stress component is usually consistent with the strain. This shows that when Y/D>0.1, the linear hypothesis basically holds. However, in the Y/D<0.1 near-wall region, the uv stress and strain present a distribution of opposite signs. On the one hand, such opposite signs phenomenon means the coefficient

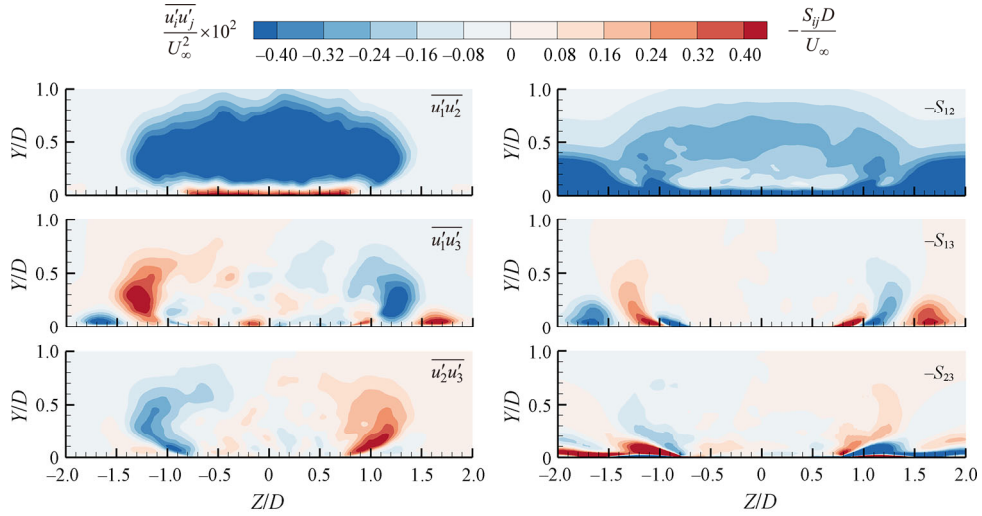

Fig. 11 Non-dimensional Reynolds stress and strain alignment at the hole exit computed with LES data

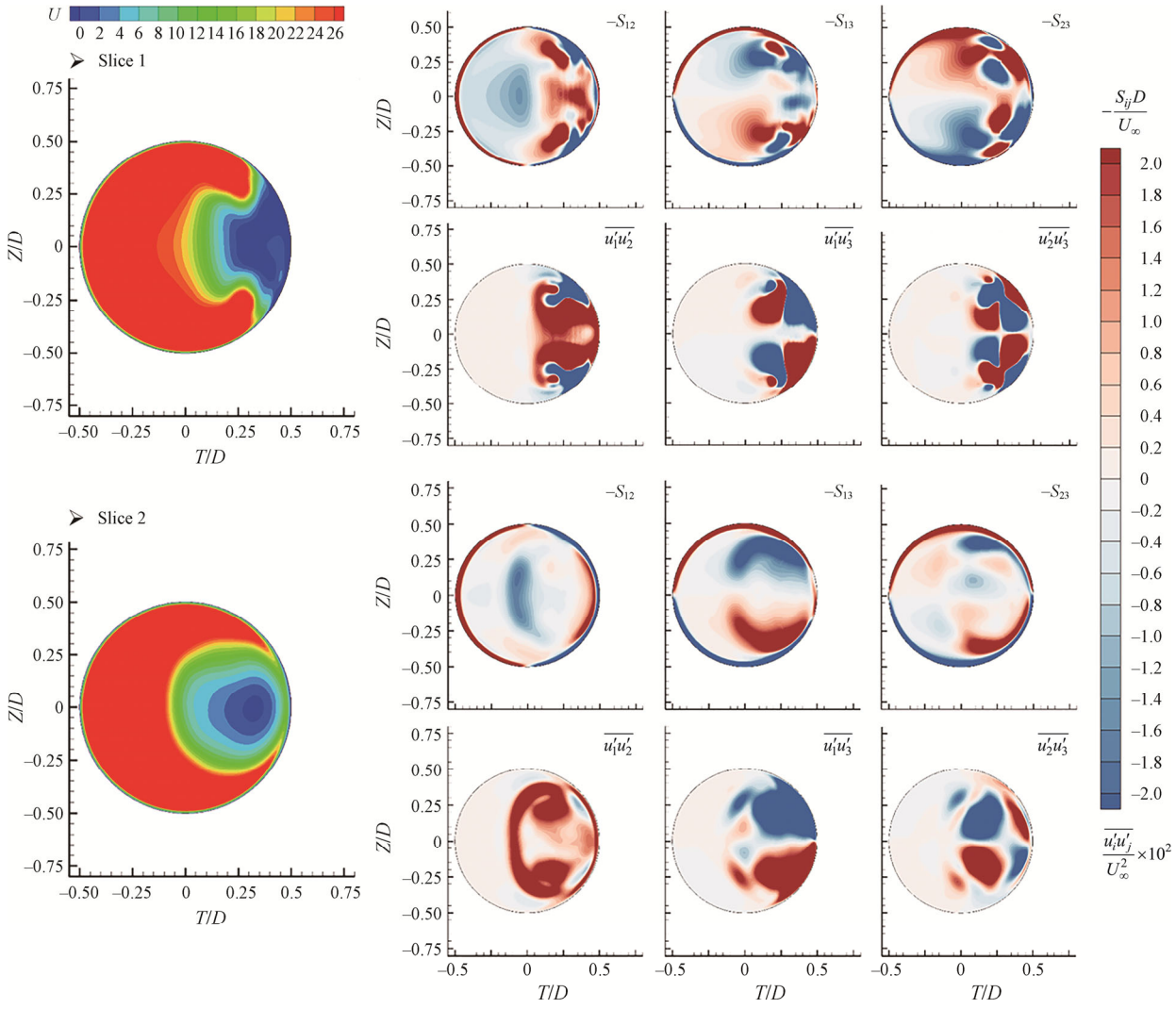

(Turn to next page)

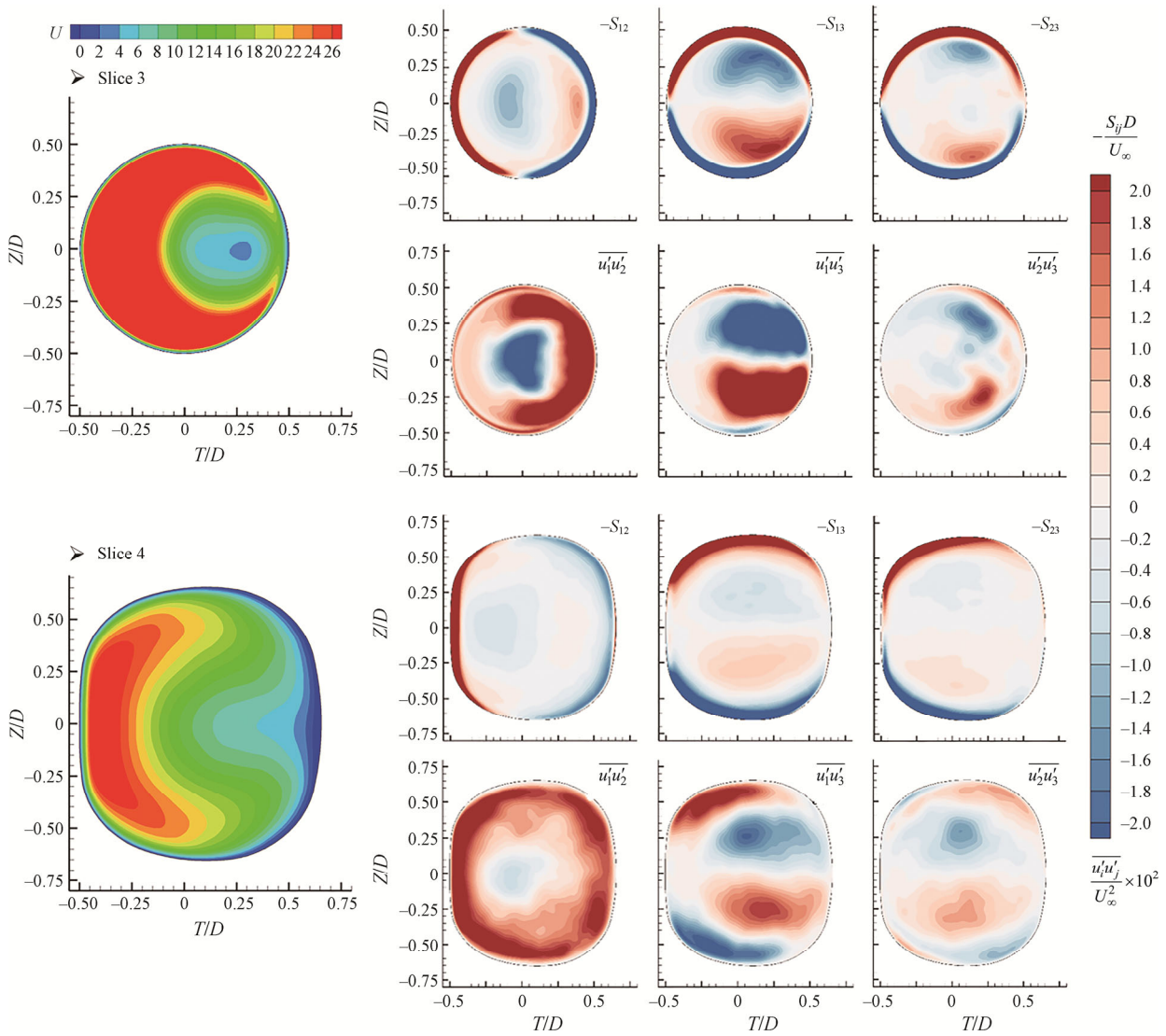

Fig. 12 Non-dimensional Reynolds stress and strain alignment with mean *X* velocity contour computed with LES data (Slice 1–4)

between the stress and strain would be negative, which is contrary to the assumption that the eddy viscosity is always positive. On the other hand, the other two shear stress and corresponding strain keep align with the same sign, which means the isotropy assumption is not exactly correct. The Reynolds stress is close to zero at the position of the CRVP in the *vw* directions, and the corresponding strain is far more than zero. Therefore, in this direction, the coefficient should be around 0, but in the same zone, there is no similar phenomenon in the *uw* direction. Such misalignment breaks the isotropy assumption again.

In terms of the in-hole flow, Fig. 12 shows the non-dimensional Reynolds stress and strain contour of Slice 1-4 shown in Fig. 8. Combined with the mean *X* velocity contour, the typical flow structure could be identified. At the inlet of the shaped hole (Slice 1), the shear stress and strain of the separation bubble appear local sign opposite phenomenon, especially in *uw* and *vw* directions. From Slice 2, it can be clearly seen that in the shear zone between the high velocity zone and the separation bubble, the signs of shear stress and strain are opposite, especially in *uv* direction. As the flow reattached to the wall, the Reynolds stress and the strain basically keep aligned in Slice 3 and Slice 4. However, in Slice 3 and Slice 4, the *uw* and *vw* stress is far different in strength with similar strain strength, which means the coefficients between stress and strain of the two directions are different.

One weakness of Boussinesq assumption is that a single eddy viscosity must be applied equally to each Reynolds stress component. However, Fig. 11 and Fig. 12 show that the single scalar eddy viscosity cannot manipulate each strain component to generate the correct Reynolds stress. According to the results of LES, although the magnitude of eddy viscosity predicted by

matching LES can be used to obtain a more accurate prediction of CRVP strength, solving the RANS equation with a single scalar eddy viscosity will produce unsatisfactory results in modelling Reynolds stress. As mentioned earlier, the assumption of scalar eddy viscosity is usually applicable, but in the near-wall zone and severely mixed shear layers it is no longer applicable. This means that the development of a turbulence model that accurately captures near-wall anisotropy can produce many improved results.

3.3 Evaluation of the gradient diffusion assumption

In addition to the eddy viscosity assumption in the flow field, there is also the gradient diffusion assumption of the heat transfer field. The rationality of constant turbulent Prandtl number can be tested by similar analysis. Fig. 13 shows the non-dimensional turbulent heat flux and temperature gradient distribution in different directions. Except for the area close to the wall, the turbulent heat flux and temperature gradient distribution in space are basically with the same sign. This shows that the temperature gradient assumption is basically valid. However, there is a phenomenon that does not conform to the assumptions at the position of the CRVP with Z/D~±(0.5–1) near the wall. In order to understand the distribution of eddy diffusion coefficient and Prandtl number intuitively, the least square method is used to solve the eddy diffusion coefficient α and turbulent Prandtl number Pr_t based on gradient diffusion assumption from the LES results according to Eq. (2) and Eq. (3):

$$\alpha_{\mathrm{tLES}} = \left[-\overline{u_i'\theta'}\left(\frac{\partial\bar{\theta}}{\partial x_i}\right)\right] \Big/ \left[\left(\frac{\partial\bar{\theta}}{\partial x_j}\right)\left(\frac{\partial\bar{\theta}}{\partial x_j}\right)\right] \tag{2}$$

$$Pr_{\mathrm{t}} = \frac{\nu_{\mathrm{tLES}}}{\alpha_{\mathrm{tLES}}} \tag{3}$$

where $\overline{u_i'\theta'}$ represents turbulent heat flux; θ is non-dimensional temperature;

In the RKE model, the turbulent Prandtl number is usually a constant approximately 0.85, but the LES results in Fig. 14 show that the Prandtl number has obvious spatial distribution characteristics, and in most of the jet area the Prandtl number is below 0.85; the Prandtl number in the near-wall area is close to 0 or even negative, and the Prandtl number in the shear area of the mainstream and coolant is about 0.2. These distributions explain the phenomenon that the misalignment of the heat fluxes and temperature gradients. The vortex diffusion coefficient reflects the eddy viscosity after being scaled by the Prandtl number. The results show that the vortex diffusion coefficient is the largest at the core of the jet and gradually decreases to the outer layer. If the assumption that the turbulent Prandtl number is a constant is used, then according to the previous scalar eddy viscosity distribution, the eddy diffusion coefficient near the wall is approximately 0, which will completely eliminate the turbulent heat flux near the wall, which does not match the actual situation. The distribution of the number shows that the normal correction will greatly help improve the accuracy of the heat transfer prediction of the RKE model.

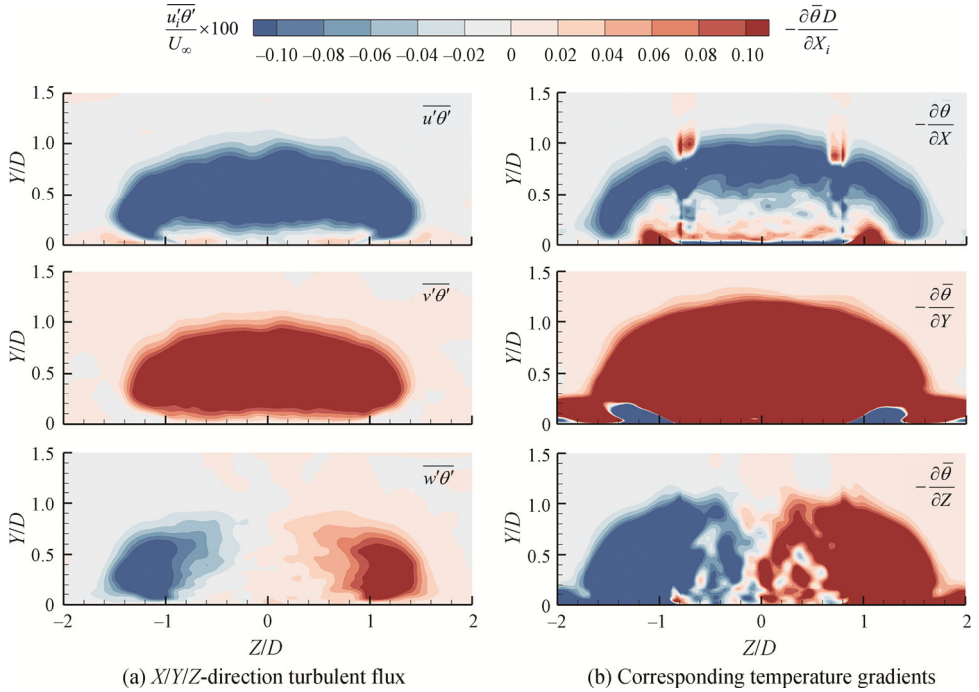

(a) $X/Y/Z$-direction turbulent flux (b) Corresponding temperature gradients

Fig. 13 Non-dimensional turbulent fluxes and temperature gradients at the hole exit computed with LES data

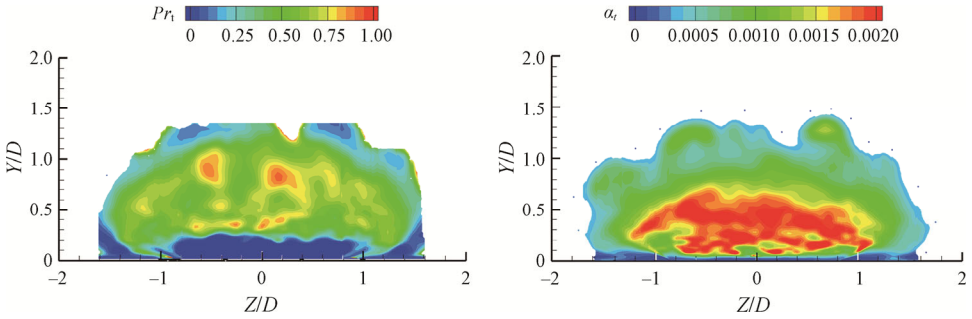

Fig. 14 Turbulent Prandtl number and eddy diffusivity at the hole exit computed with LES data

3.4 Analysis of in-hole flow mechanism

In order to explore the in-hole flow mechanism, the flow field in the shaped hole is extracted and analysed with iPOD. This is a tool by math process to extract the key flow field structure of unsteady flow for mechanism analysis, flow field reconstruction and flow control. The adopted iPOD is the improved version of POD, which is more suitable for large scale data process [13]. The most typical modals related to energy of the phenomena can be captured. With 2308 snapshots, which is corresponding to two passing periods, 50 modes are outputted. Their energy ratios are computed based on the singular value of each mode. As shown in Fig. 15, the Mode0, which represents the time-averaged flow-field, occupies more than 90% energy. In the rest modes, the Mode1 contributes to the unsteady flow far more than others. From mode15, the single mode contributes less than 0.1%.

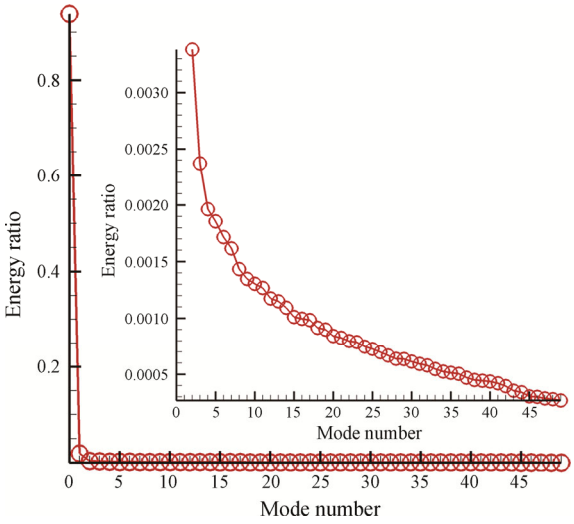

Fig. 15 The energy ratio of each mode

Due to the approximate process in iPOD, the validation is necessary. Fig. 16 shows the X velocity contour of Mode0, which is consistent with the LES time-averaged results shown in Fig. 8. Therefore, the iPOD results are reliable. According to the formula Eq. (4) used in iPOD, the Reynolds stress can be obtained by adding up the Reynolds stress of each mode and then averaging them as Eq. (5). Relevant derivation is as following:

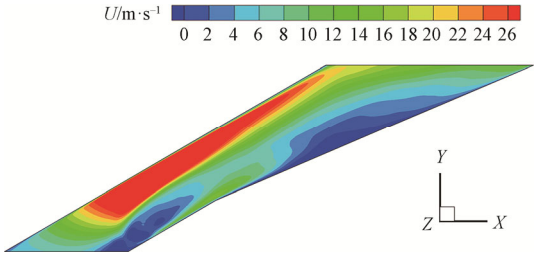

Fig. 16 The X velocity contour of Mode0

$$A=\begin{bmatrix} u_{1,1} & u_{1,2} & \cdots & u_{1,N} \\ u_{2,1} & u_{2,2} & \cdots & u_{2,N} \\ \vdots & \vdots & \vdots & \vdots \\ u_{M,1} & u_{M,2} & \cdots & u_{M,N} \\ v_{1,1} & v_{1,2} & \cdots & v_{1,N} \\ v_{2,1} & v_{2,2} & \cdots & v_{2,N} \\ \vdots & \vdots & \vdots & \vdots \\ v_{M,1} & v_{M,2} & \cdots & v_{M,N} \\ w_{1,1} & w_{1,2} & \cdots & w_{1,N} \\ w_{2,1} & w_{2,2} & \cdots & w_{2,N} \\ \vdots & \vdots & \vdots & \vdots \\ w_{M,1} & w_{M,2} & \cdots & w_{M,N} \end{bmatrix} = U\sum V = \Phi V \tag{4}$$

$$\begin{aligned} \overline{u_i' u_{i+\alpha M}'} &= \frac{1}{N}\sum_j A_{i,j}A_{i+\alpha M,j} \\ &= \frac{1}{N}\sum_l \left(\sum_k \Phi_{i,k}V_{k,j}\right)\left(\sum_n \Phi_{i+\alpha M,n}V_{n,j}\right) \\ &= \frac{1}{N}\sum_k\sum_n \Phi_{i,k}\Phi_{i+\alpha M,n}\sum_n V_{k,j}V_{n,j} \\ &= \frac{1}{N}\sum_k \Phi_{i,k}\Phi_{i+\alpha M,k} \end{aligned} \tag{5}$$

where A contains the velocity components of M points in N instants.

By adding up the first 32 modes, the results basically converge compared with the LES results as shown in Fig. 17. It is worthy noticing that the contour of Mode 1 is

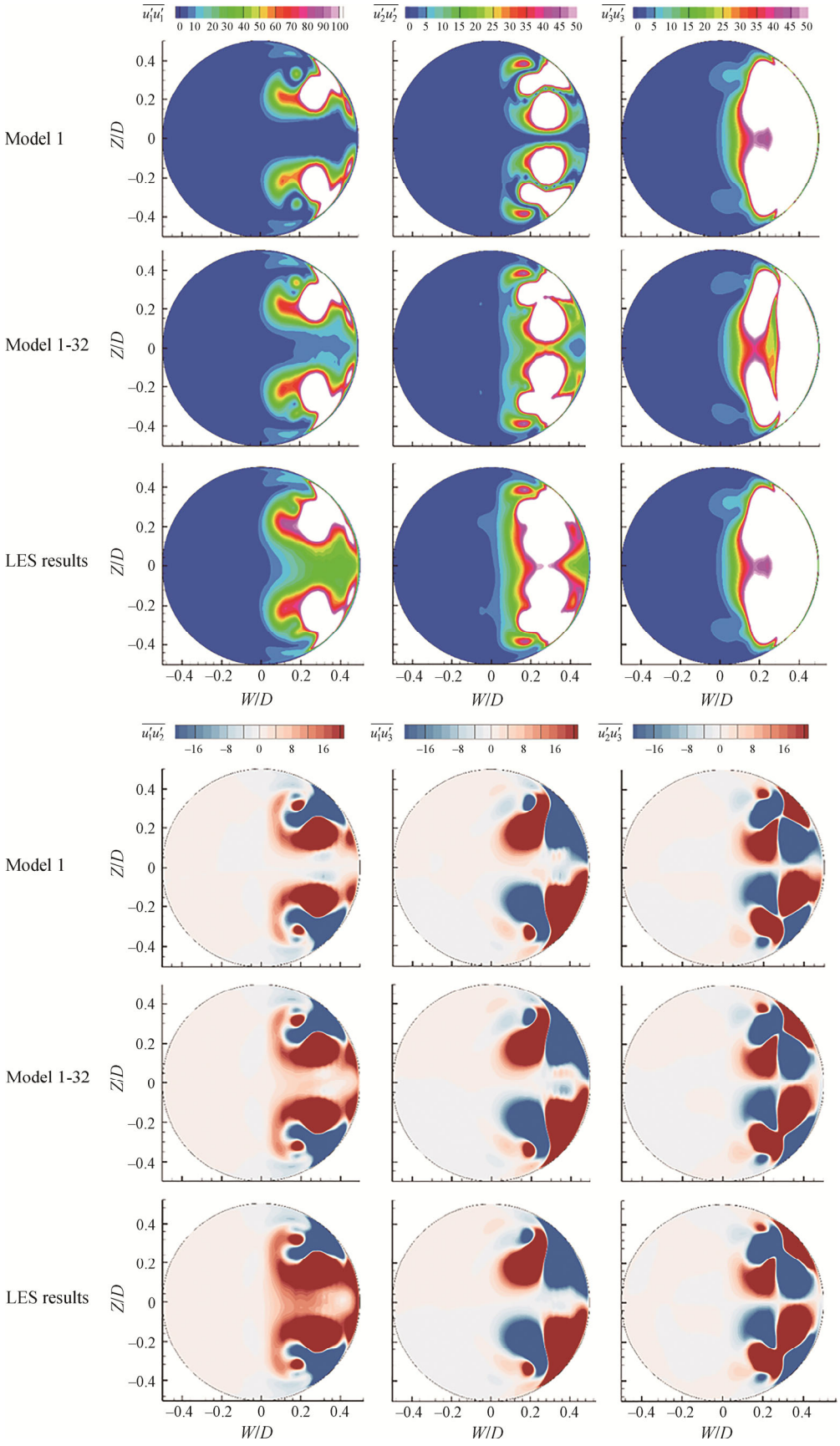

Fig. 17 Reynolds stress contour of Mode 1, Mode 1-32, and LES results of Slice 1

already similar to the LES results. After calculation, the area-averaged value of $\overline{u_1'u_1'}$, $\overline{u_2'u_2'}$, $\overline{u_3'u_3'}$ in Mode1 occupies more than 60% of the LES results, which means the dominant unsteady flow structure has been captured by Mode1. Combined with the non-dimensional turbulent kinetic energy contour shown in Fig. 9, it is obviously that the turbulent energy concentrates on three zones, including the inlet separation bubble, the diffusion section separation bubble, and the shear zone between the high velocity zone and the separation zone. From the fluctuation velocity contour of Mode1 shown in Fig. 18, it can be deduced that the inlet separation bubble is corresponding to the Z direction velocity fluctuation, while the diffusion section separation bubble and the shear zone corresponding to the X direction velocity fluctuation.

Besides Mode1, several other modes present typical character. In Fig. 19, there are one or more dominant character frequencies appearing in Fast Fourier Transformation (FFT) results of Mode 3, Mode 4, Mode 8, Mode 9, Mode 12 and Mode 14. Correspondingly, in the Z direction fluctuation velocity contour, there are similar profiles appearing along the streamline. Naturally, it is deduced that there exists some convection flow introduced from the shear zone. Four monitored points are set up in the shaped hole shown in the Fig. 20. All of them are located in the shear zone.

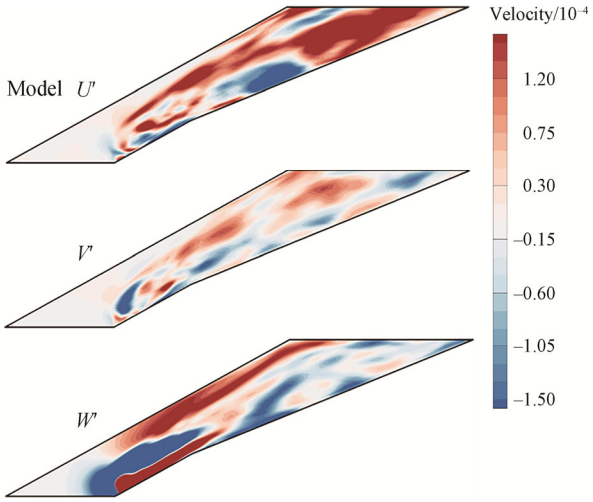

Fig. 18 Fluctuation velocity contour of Mode1

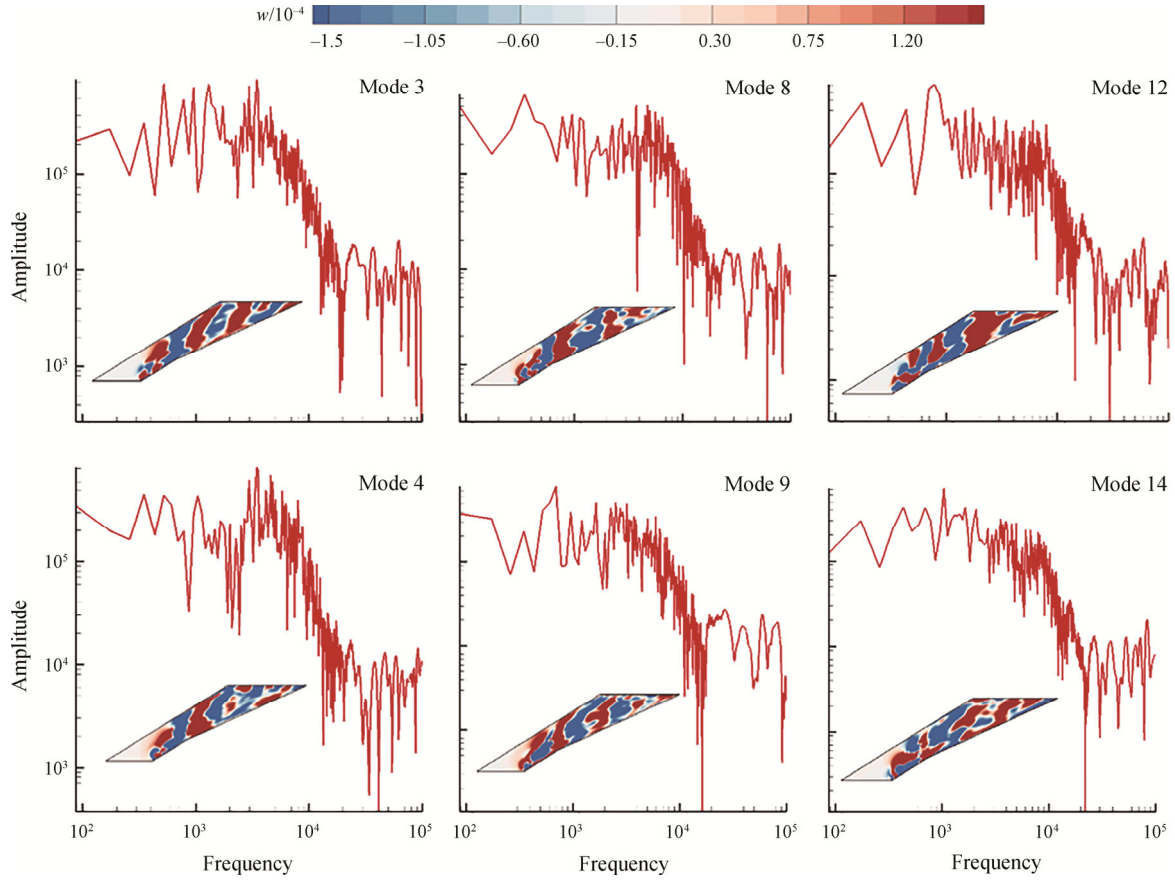

Fig. 19 FFT over POD coefficients at each sampling time with corresponding Z direction fluctuation velocity contour

The FFT results of the four monitored points are shown in Fig. 21, where the frequency is normalized by the hole diameter and the mainstream velocity according to Eq. (6):

$$\text{Strouhal number} = fD/U_{\infty} \tag{6}$$

Firstly, the existence of the dominant frequency at each point confirms previous guess. Furthermore, it is noticed that the frequency and the amplitude decrease along the streamline (from Point 0 to Point 3). The frequency decreases nearly the half of the origin from the Point 0 with 0.93 to the Point 3 with 0.52.

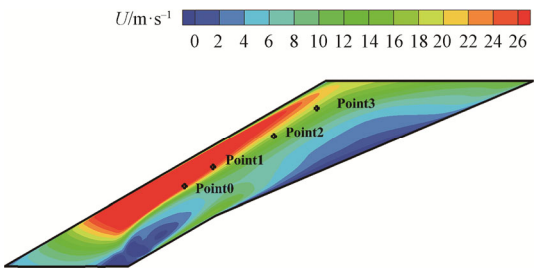

Fig. 20 Positions of the monitored points

In order to distinguish the anisotropy turbulence characteristic, the flow field in the shaped hole is analysed with the Lumley triangle. The results are shown in Fig. 22; the purple points include all the points in the hole except the boundary layer. The distribution is basically random and far away from the origin point, which means the turbulence is basically anisotropy. Some interesting phenomena appear when the flow filed is divided into several zones according to the flow structure. Firstly, the turbulence in the inlet zone is basically dominated by two components, while that in the outlet zone is basically dominated by one component. Furthermore, in the zone 2, which is shaded by red colour beside the inlet separation bubble, the turbulence remains the characteristic with two components. Then things change when the flow begins to speed up due to the expansion of the separation bubble. The flows of the blue points of the zone 1 are mostly dominated by one component. The zone 1 includes the high-speed zone and the shear zone. It is deduced that in the high-speed zone, the turbulence intensity is weaken, so that the turbulence degenerates. In the shear zone, one possible reason for such characteristic is the convection flow structure linked with previous observation.

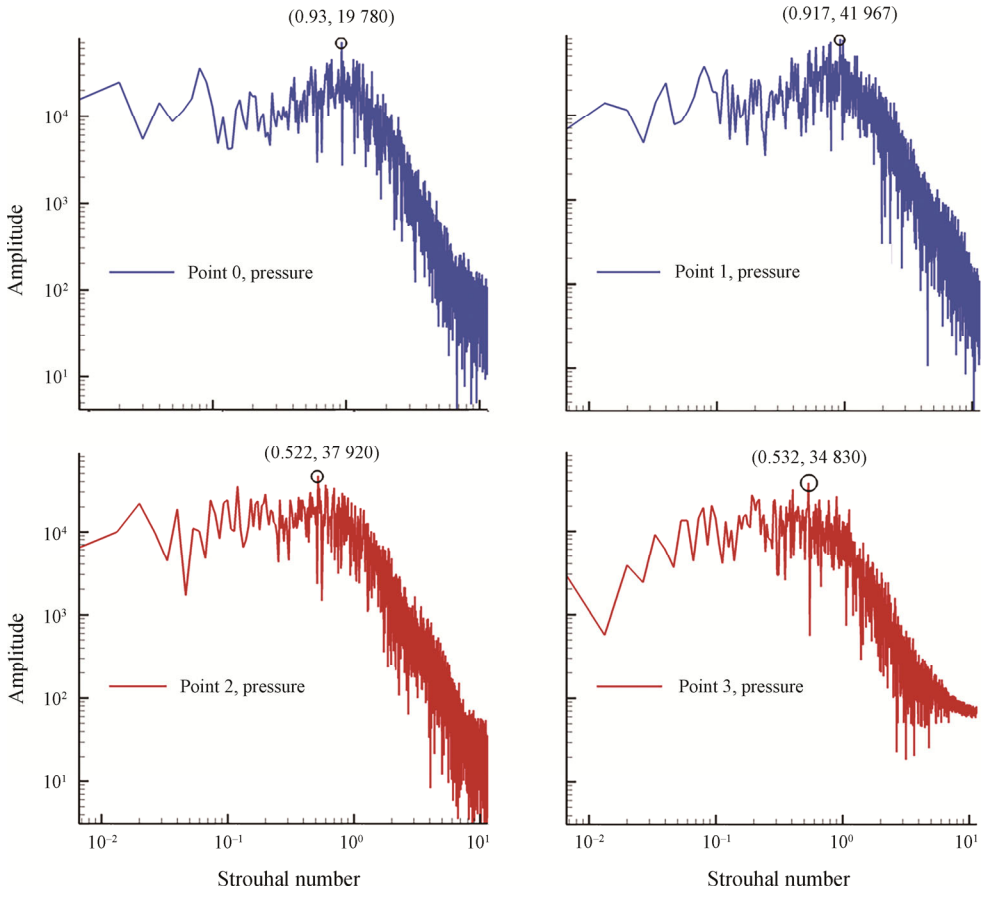

Fig. 21 FFT over pressure signal at the monitored points

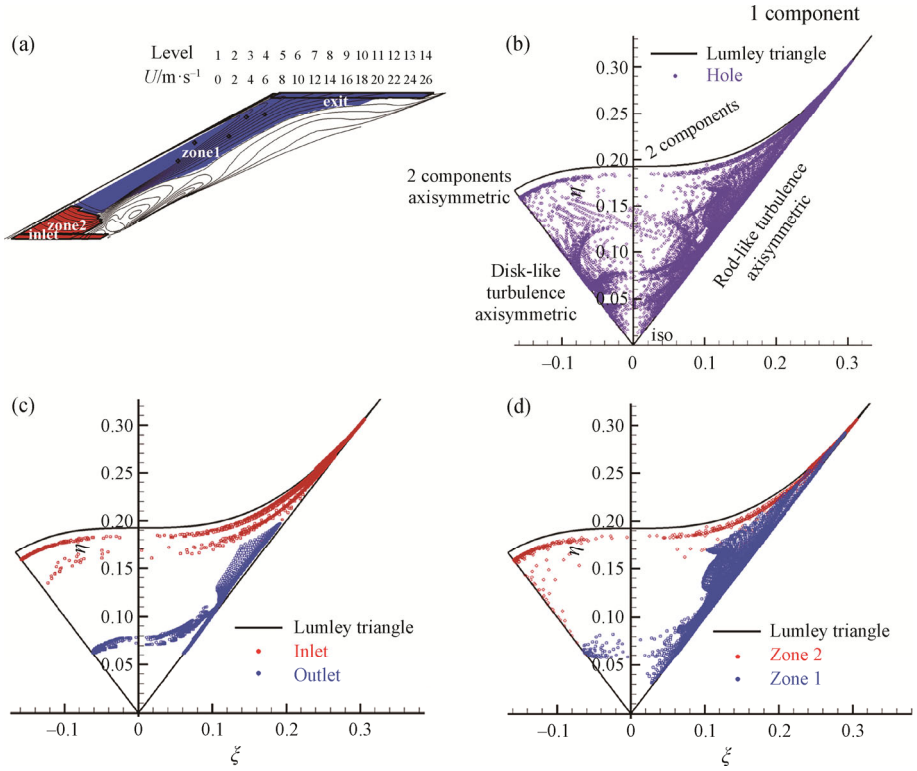

Fig. 22 Turbulence characteristic of the in-hole flow reflected by the Lumley triangle

4. Conclusions

In this study, numerical simulations based on LES and RANS are performed to assess the turbulence characteristics of shaped film cooling hole.

The weaknesses of the RANS turbulence model (RKE) in predicting the film cooling of shaped hole is evaluated. The results show that RKE model does not have sufficient prediction of the spatial distribution profile of eddy viscosity as well as the turbulent kinetic energy. LES data is used to evaluate the Boussinesq hypothesis and the gradient diffusion hypothesis. Finally, the in-hole flow mechanism is analysed in detail. The main conclusions are as following:

(1) In the near-wall area (Y/D<0.1), the stress and strain with opposite signs appears, and the single scalar eddy viscosity near the wall is not reasonable. The correction of the scalar eddy viscosity must be considered in the near-wall region.

(2) The turbulent Prandtl number needs to be changed in space, especially along the normal direction.

(3) Some convection flow structure is induced from the in-hole shear zone, and the frequency and amplitude decays along the streamline.

(4) The anisotropy characteristics of in-hole flow concentrate on typical flow zone, which has guiding significance for modelling the film cooling.

Acknowledgements

This study is supported by the National Natural Science Foundation of China (Project Grant No. 51876098) and National Science and Technology Major Project (J2019-III-0007-0050). This research is also sponsored by the Open Fund from Science and Technology on Thermal Energy and Power Laboratory (TPL2018B05).

References

[1] Bogard D.G., Thole K.A., Gas turbine film cooling. Journal of Propulsion and Power, 2006, 22(2): 249–270.

[2] Goktepeli I., Atmaca U., Cakan A., Investigation of heat transfer augmentation between the ribbed plates via taguchi approach and computational fluid dynamics. Journal of Thermal Science, 2020, 29: 647–666.

[3] Galeazzo F., Donnert G., Habisreuther P., Zarzalis N., Valdes R.J., Krebs W., Measurement and simulation of turbulent mixing in a jet in crossflow. ASME. Journal of Engineering for Gas Turbines and Power, 2011, 133(6): 061504.

[4] Laroche E., Fenot M., Dorignac E., Vuillerme J.J., Brizzi, L.E., Larroya J.C., A combined experimental and numerical investigation of the flow and heat transfer

inside a turbine vane cooled by jet impingement. Journal of Turbomachinery, 2018, 140(3): 031002.

[5] Foroutan H., Yavuzkurt S., Numerical simulations of the near-field region of film cooling jets under high free stream turbulence: Application of rans and hybrid urans/large eddy simulation models. Journal of Heat Transfer, 2015, 137(1): 011701.

[6] Bergeles G., Gosman A.D., Launder B.E., The turbulent jet in a cross stream at low injection rates: a three-dimensional numerical treatment. Numerical Heat Transfer, Part B: Fundamentals, 1978, 1(2): 217–242.

[7] Lakehal D., Near-wall modeling of turbulent convective heat transport in film cooling of turbine blades with the aid of direct numerical simulation data. Journal of Turbomachinery, 2002, 124(3): 485–498.

[8] Bianchini C., Andrei L., Andreini A., Facchini B., Numerical benchmark of nonconventional RANS turbulence models for film and effusion cooling. Journal of turbomachinery, 2013, 135(4): 041026.

[9] Ling J., Ruiz A., Lacaze G., Oefelein J., Uncertainty analysis and data-driven model advances for a jet-in-crossflow. Journal of Turbomachinery, 2017, 139(2): 021008.

[10] Sarkar S., Babu H., Large eddy simulation on the interactions of wake and film-cooling near a leading edge. Journal of Turbomachinery, 2014, 137(1): 011005.

[11] Stratton Z.T., Shih T.I.P., Identifying weaknesses in eddy-viscosity models for predicting film cooling via large-eddy simulations. Journal of Propulsion and Power, 2019, 35(3): 583–594.

[12] Schroeder R.P., Thole K.A., Adiabatic effectiveness measurements for a baseline shaped film cooling hole. Proceedings of the ASME Turbo Expo 2014: Turbine Technical Conference and Exposition. Volume 5B: Heat Transfer, 2014. V05BT13A036. ASME. DOI: 10.1115/GT2014-25992.

[13] Wang Q.S., Su X.R., Yuan X., Large-eddy simulation of shaped hole film cooling with the influence of cross flow. International Journal of Turbo & Jet-Engines. 2020, pp. 000010151520200012. DOI: 10.1515/tjj-2020-0012.